Electronic Supplementary Information (ESI)

The impact of size effects on the electrochemical behaviour of Cu_2O-coated Cu nanopillars for advanced Li-ion microbatteries

Mario Valvo[*,§], David Rehnlund[§], Ugo Lafont[#], Maria Hahlin[§], Kristina Edström[§], and Leif Nyholm[*,§]

[§]Department of Chemistry-Ångström, The Ångström Laboratory, Uppsala University, Box 538, 75121 Uppsala, Sweden.

[#]Novel Aerospace Materials, Aerospace Engineering, Delft University of Technology, 2629 HS Delft, The Netherlands.

**Corresponding authors:* Mario.Valvo@kemi.uu.se, Leif.Nyholm@kemi.uu.se

S.1. Calculation of the geometrical area gain factor and resistance for the pillars

The geometrical area gain factor, Γ, for the 3D substrate was calculated using the following equation:

$$\Gamma = N \cdot (2\pi r h) \qquad \text{(S1)}$$

where N denotes the average numerical density of pillars per unit area, r their mean radius and h their average height. Note that in this calculation the nanopillars were hence treated as ideal, smooth cylinders, neglecting any surface roughness.

The electrical resistance of an ideal cylindrical Cu pillar, R_{pil}, was evaluated by Ohm's first law:

$$R_{pil} = \rho_{Cu} \frac{h}{A} \qquad \text{(S2)}$$

where A is the cross-section area, h the typical height and ρ_{Cu} the room temperature resistivity of copper. A similar calculation was used to determine the resistance of the thin active layer (i.e. Cu_2O) covering the entire 3D substrate area.

S.2. Calculation of the amounts of Cu_2O and Fe_2O_3 in the infiltrated/pyrolyzed electrode

The amount of Cu_2O on the surface of the infiltrated/pyrolyzed electrode was estimated to be 0.97 mg based on an electrode area of 108 cm^2 (i.e. a footprint area of 1.8 cm^2 and a gain factor of 60), a Cu_2O layer thickness of 15 nm and a Cu_2O density of 6.0 g cm^{-3}. This amount of Cu_2O corresponds to a charge of about 0.36 mAh, given a theoretical specific capacity for Cu_2O of 375 mAh g^{-1}.

The amount of iron oxide in the ultimate coating was estimated based on the volume and the concentration of the solution used in the infiltration step. Considering approximately 25 µl of the 1 g L^{-1} Fe(II) acetate solution, the maximum amount of Fe_2O_3 in the final coating after pyrolysis should be about 12 µg. Based on the theoretical capacity of 1007 mAh g^{-1} for Fe_2O_3, this corresponds to a maximum contribution to the overall charge of about 0.012 mAh. This contribution merely accounts for about 3% of the total capacity, which is why the practical (i.e. experimental) capacity of the infiltrated/pyrolyzed electrode was ascribed entirely to Cu_2O.

S.3. Calculation of the standard potentials for the conversion of Cu_2O and Fe_2O_3

The standard potentials for the reductions of bulk Cu_2O (ΔG^0= -146.0 kJmol^{-1}) and Fe_2O_3 (ΔG^0= -742.2 kJmol^{-1}) producing Li_2O (ΔG^0= -561.2 kJmol^{-1}) and the associated metals, as indicated below:

$$Cu_2O + 2Li^+ + 2e^- \leftrightarrow Li_2O + 2Cu \quad \text{(S3)}$$

$$Fe_2O_3 + 6Li^+ + 6e^- \leftrightarrow 3Li_2O + 2Fe \quad \text{(S4)}$$

were calculated, yielding respectively 2.1 and 1.6 V *vs.* Li^+/Li on the basis of the equation $\Delta G = -nFE$.

S.4. Calculation of the standard potential shift due to the presence of nanoparticles

The change in the standard potential as a function of the radius of the nanoparticles can be approximated using the following expression:[S1]

$$E_p^0 = \left(E_{bulk}^0 - \frac{2\gamma V_M}{nFr} \right) \quad \text{(S5)}$$

where E^0_p and E^0_{bulk} denote the respective standard electrode potentials for a particle and its related *bulk* material, γ and r refer to the surface tension and the radius of the particle, respectively, whereas V_M represents the molar volume of the bulk material, n the number of electrons involved in the redox reaction and F is the Faraday constant.

By assuming the presence of copper nanoparticles with $\gamma \approx 2$ J m^{-2} (as it has been reported for small gold nanoparticles[S2]), $r \approx 60$ nm, $V_M \approx 7.09$ cm^3 mol^{-1} (for bulk Cu) and $n = 1$ (i.e. assuming an oxidation of Cu to Cu$^+$), a negative shift in the standard potential of merely ≈6 mV is obtained. As negative shifts of about 60, 290 and 980 mV are respectively introduced by assuming particle radii of 5, 1 and 0.3 nm, it is clear that the generation of a distribution of nanoparticles with different sizes by electrochemical milling may indeed give rise to a significantly extended potential window. This conclusion is also in excellent agreement with recent findings regarding the electrochemical behaviour of gold and silver nanoparticles.[S1,S2]

It should be noted that also the surface tension γ becomes size-dependent for very small particle sizes and that it is further affected by different crystal orientations. Therefore, different nanoparticles having distinct sizes below a certain critical threshold, for which γ is no longer constant and becomes function (e.g. $\gamma = \gamma(r)$) of the particle radius (as for the simplest case of a spherical, amorphous nanoparticle), will also have varying surface tensions. It is, nevertheless, still instructive to use a constant reference value (i.e. $\gamma \approx 2$ J m^{-2}), derived from experimental observations of small (i.e. $r < 2$ nm) metal particles,[S2] for the estimation of the shift in the standard potential, since the analytical expression of $\gamma = \gamma(r)$ is not known a priori for the Cu nanoparticles.

S.5. Supplementary figures

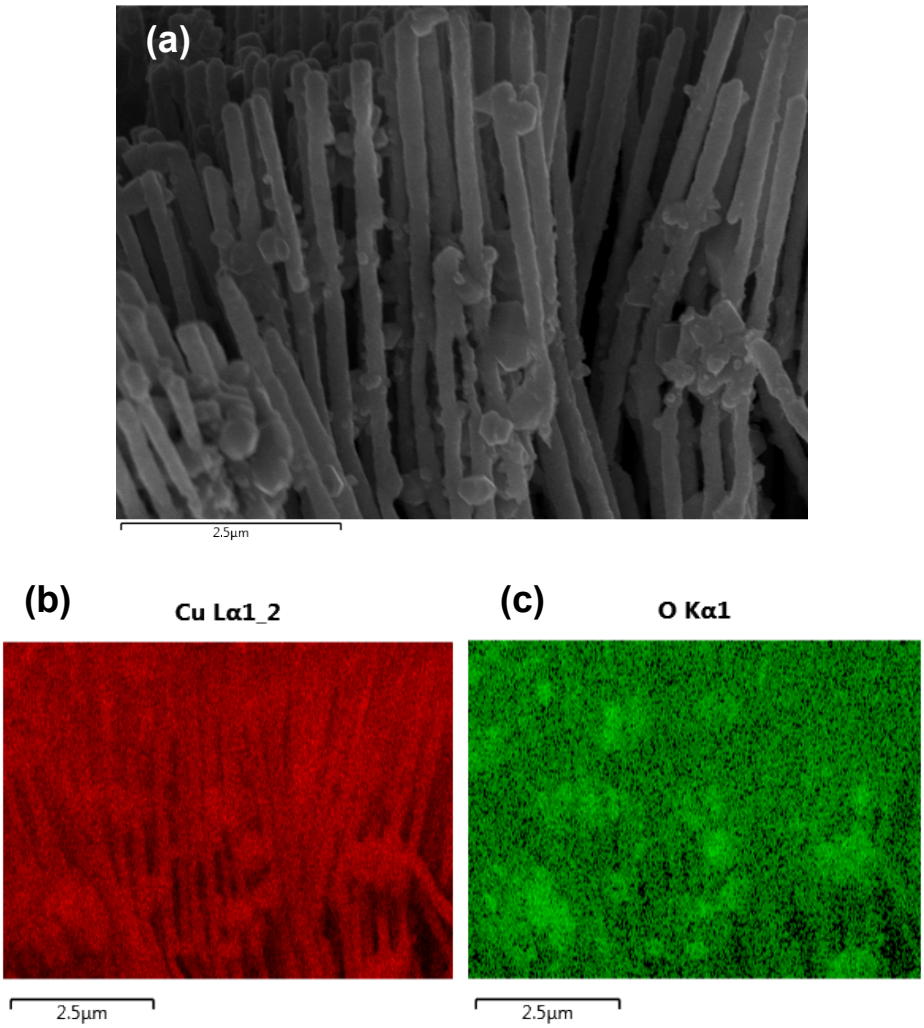

Figure S1. a) SEM cross-section micrograph displaying the morphology of the crystal-like deposits on the surface of the 3D electrode after the infiltration and pyrolysis steps. b) and c) show chemical maps for copper and oxygen, respectively, obtained in connection with the SEM image in a). A close comparison of these maps indicates that the electrode surface contained mainly Cu_2O.

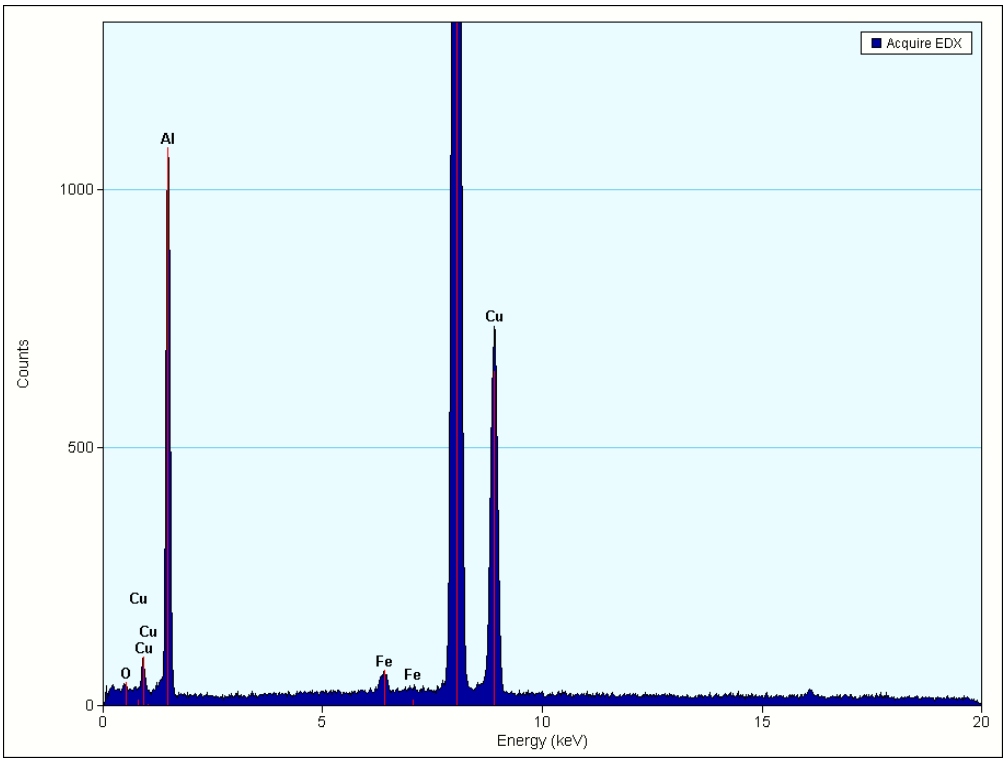

Figure S2. EDS spectrum obtained for the region depicted in the TEM micrograph in Fig. 4c. The strong Al peak was due to the Al grid support of the TEM sample holder.

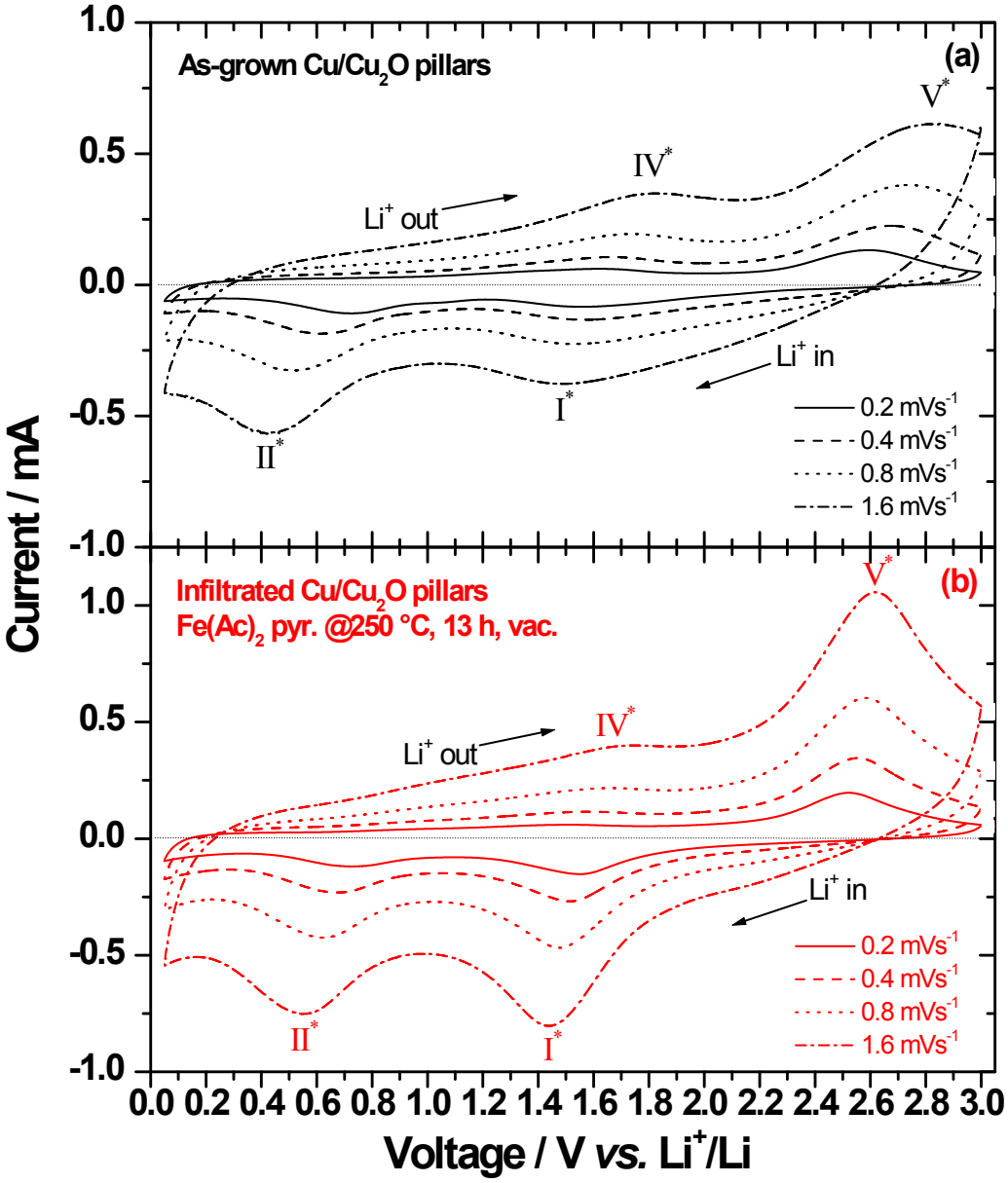

Figure S3. Cyclic voltammograms recorded between 0.05 and 3.0 V *vs.* Li^+/Li for a) the pristine and b) the infiltrated/pyrolyzed electrode using increasing scan rates from 0.2 to 1.6 mVs^{-1}. The asterisks denote that the peaks in all the voltammograms were obtained after the first cycle. Note that the voltammogram in a) has been obtained after previous galvanostatic cycling of the as-grown Cu_2O-coated electrode.

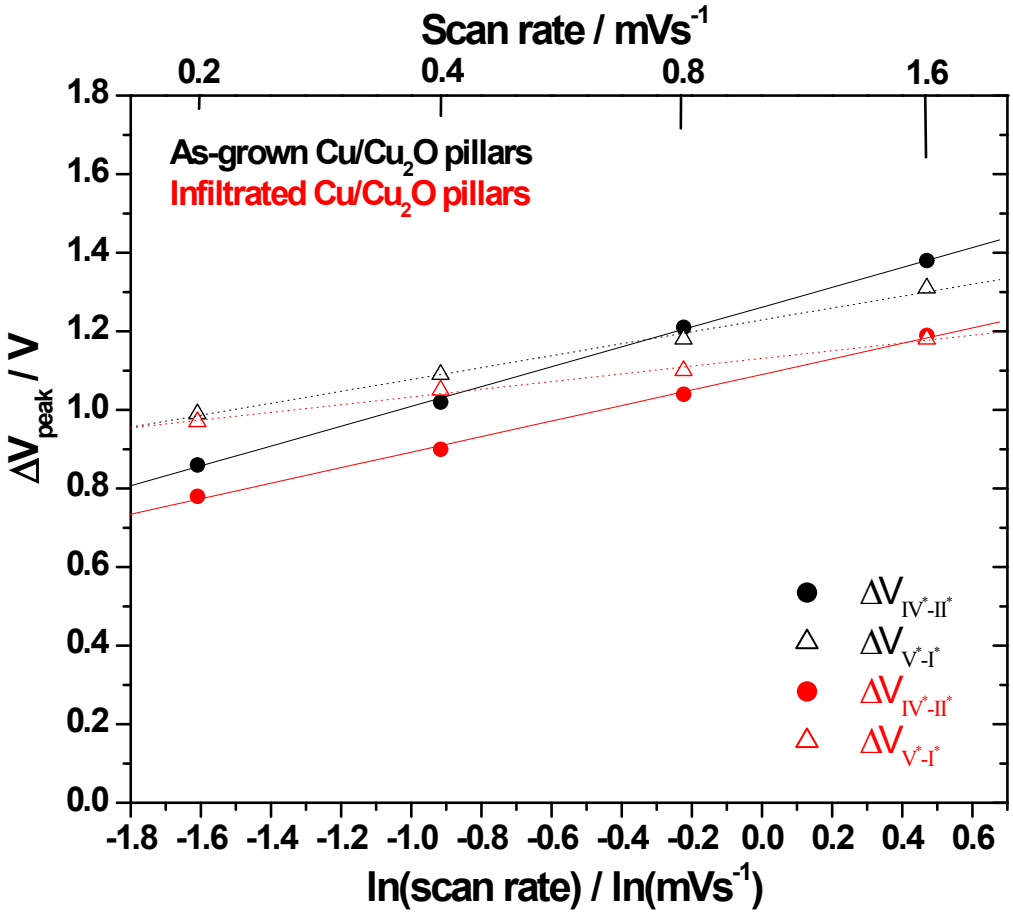

Figure S4. Plots of the peak potential difference between peaks V* and I*, as well as between peaks IV* and II*, as a function of the logarithm of the scan rate for the pristine (black symbols) and infiltrated/pyrolyzed (red symbols) electrodes. The data points have been extracted from the previous voltammograms. The top scale in the graph indicates the actual scan rates. The asterisk-marked peaks denote features obtained after the first cycle.

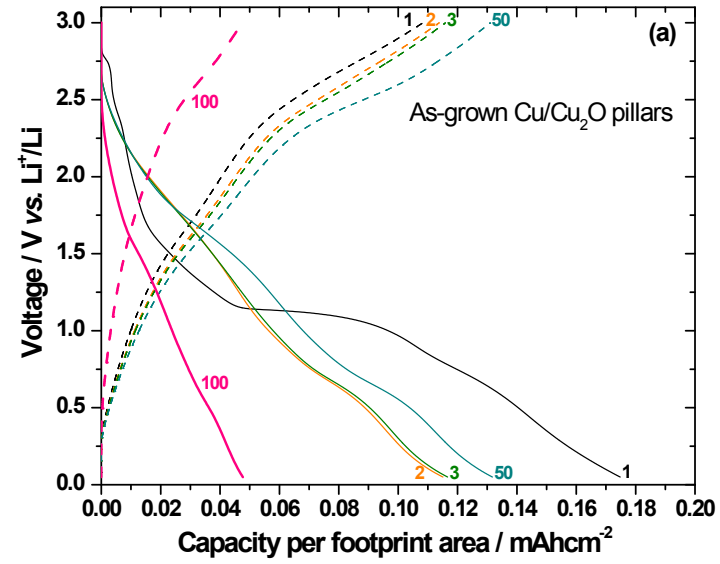
(a)
As-grown Cu/Cu2O pillars
Voltage / V vs. Li+/Li
Capacity per footprint area / mAhcm-2
1
2
3
50
100

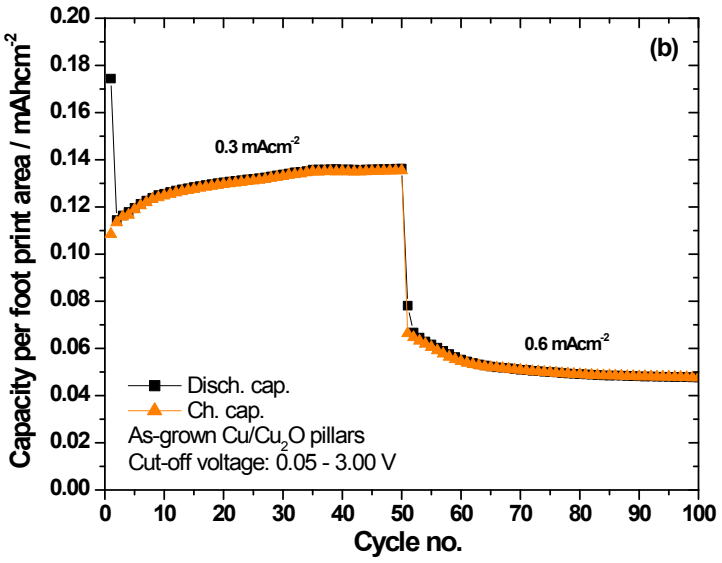
(b)
0.3 mAcm-2
0.6 mAcm-2
Disch. cap.
Ch. cap.
As-grown Cu/Cu2O pillars
Cut-off voltage: 0.05 - 3.00 V
Capacity per foot print area / mAhcm-2
Cycle no.

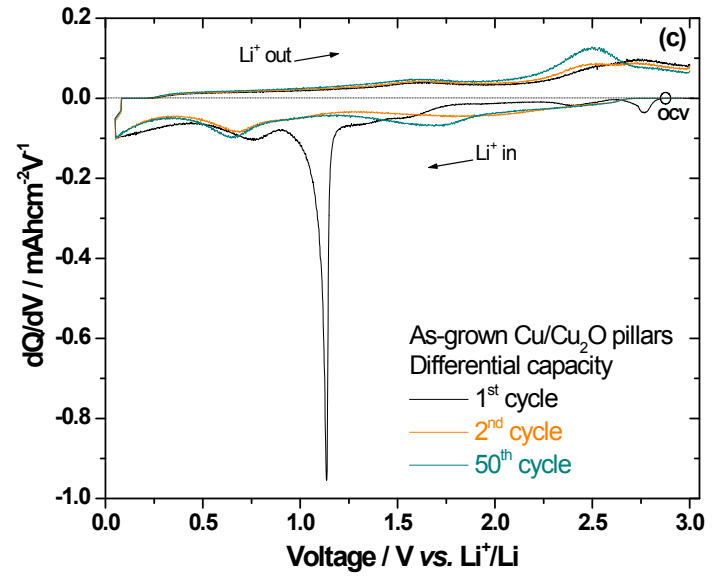
(c)
Li+ out
Li+ in
ocv
As-grown Cu/Cu2O pillars
Differential capacity
1st cycle
2nd cycle
50th cycle
dQ/dV / mAhcm-2V-1
Voltage / V vs. Li+/Li

Figure S5. a) chronopotentiograms showing different charge/discharge cycles for the pristine Cu_2O-coated electrode obtained with a current density of 0.3 or 0.6 mA cm^{-2} (the thicker curves labelled '100' were attained at 0.6 mA cm^{-2}) between 0.05 and 3.0 V *vs*. Li^+/Li. The solid lines refer to discharge (i.e. reduction), whereas the dashed ones correspond to charge (i.e. oxidation). Note the irreversible contribution due to SEI formation on the initial discharge. b) charge and discharge capacities as a function of the cycle number for the pristine 3D electrode. c) differential capacity plot obtained for some of the charge/discharge curves at 0.3 mA cm^{-2} shown in a). Note the shape similarity of the initial cycles with those of the cyclic voltammograms for the infiltrated/pyrolized Cu/Cu_2O electrode presented in Fig. 5 in the main text.

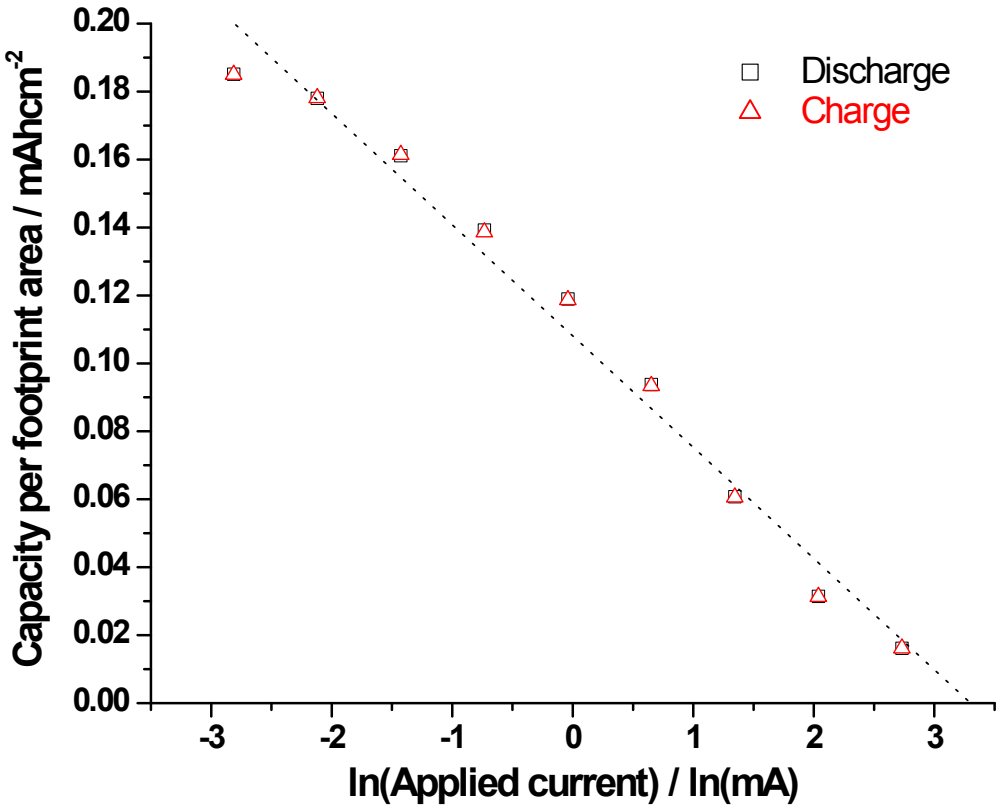

Figure S6. Obtained capacities per footprint area for the infiltrated/pyrolyzed 3D electrode *vs.* the logarithm of the applied current upon galvanostatic cycling at different current densities. The data were extracted from Fig. 6c. Note the overall linear trend for the data points.

Figure S7. Photo of the airbrush pen and the iron acetate solution used for aerosol generation and infiltration of the as-electrodeposited 3D current collector. The inset is a photo showing the 3D current collector after the infiltration and pyrolysis processes.

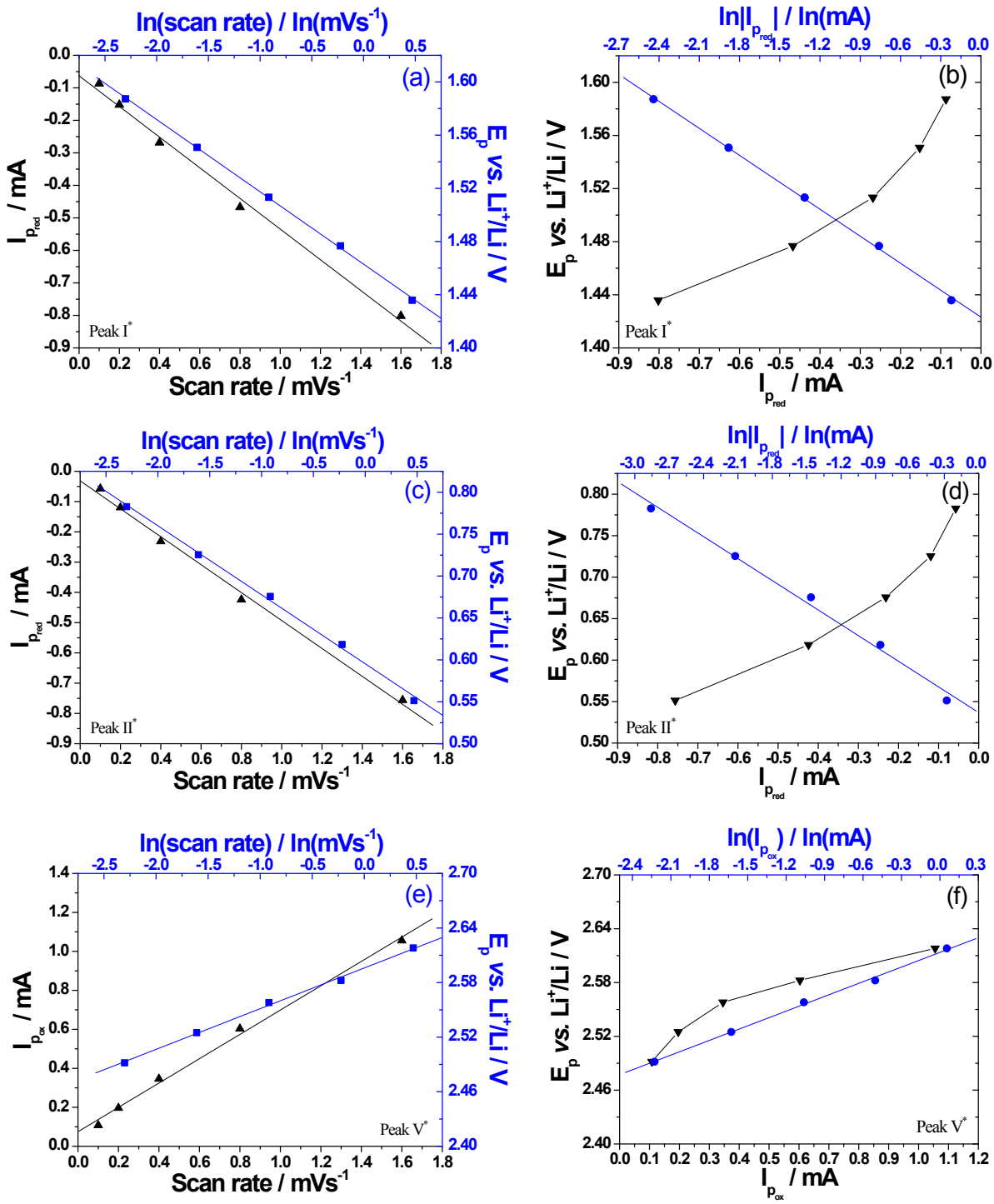

Figure S8. Plots showing the behaviour of peak currents and peak potentials as respective functions of the scan rate and the logarithm of the scan rate (a, c and e) for the initial CV cycles of the infiltrated/pyrolyzed electrode. All data points were extracted from Fig. 5 and Fig. S3b. The evolution of the peak potentials with their related peak currents (b, d and f) is reported as well. Note the linear

behaviour of the peak currents with the applied scan rates for both reduction (I^*, II^*) and oxidation (V^*) features, whereas a logarithmic trend for the same peak potentials *vs.* both the scan rates and the current peaks is observed. The linear relationship of I_p with the scan rate indicates that Li^+ uptake/release occurred under thin layer electrochemical conditions, whereas the logarithmic dependences suggest that limitations in the electron transfer kinetics were present, due to major structural changes upon conversion and deconversion of Cu_2O.

S.6. Supplementary references

S1. P. L. Redmond, A. J. Hallock, L. E. Brus, *Nano Lett.*, 2005, **5**, 131.

S2. R. A. Masitas, F. P. Zamborini, *J. Am. Chem. Soc.*, 2012, **134**, 5014.